Materials and Design 198 (2021) 109300

Contents lists available at ScienceDirect

Materials and Design

journal homepage: www.elsevier.com/locate/matdes

Ca ions chelation, collagen I incorporation and 3D bionic PLGA/PCL electrospun architecture to enhance osteogenic differentiation

Xuefeng Zhou [a], Xi Cheng [b], Danlei Xing [b], Qi Ge [b], Yan Li [a], Xianghong Luan [c], Ning Gu [a,**], Yunzhu Qian [b,*]

[a] State Key Laboratory of Bioelectronics, Jiangsu Key Laboratory for Biomaterials and Devices, School of Biological Science and Medical Engineering, Southeast University, Nanjing 210096, People's Republic of China
[b] Center of Stomatology, the Second Affiliated Hospital of Soochow University. Suzhou 215004, People's Republic of China
[c] Texas A&M Center for Craniofacial Research and Diagnosis, Dallas, TX 75246, United States of America

HIGHLIGHTS

- Collagen I-incorporated PLGA/PCL matrix was electrospun into 3D scaffolds.
- ECM-like architecture chelated by Ca ions via polydopamine coating for local delivery.
- Chelated-Calcium synergistically with collagen I promoted osteogenesis.

GRAPHICAL ABSTRACT

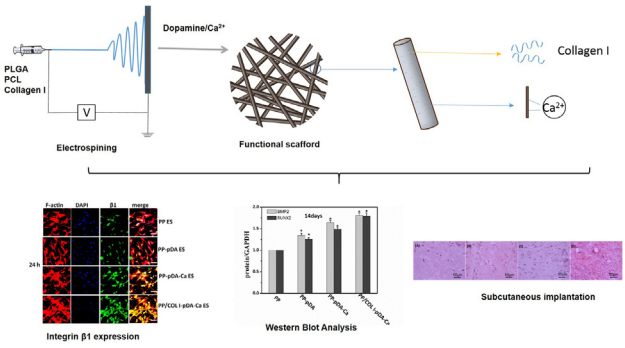

ARTICLE INFO

Article history:
Received 28 June 2020
Received in revised form 26 October 2020
Accepted 5 November 2020
Available online 6 November 2020

Keywords:
Osteogenesis
Ca ions
Collagen I
Bone regeneration
Electrospinning scaffolds

ABSTRACT

Bioactive synthetic scaffolds with 3D porous structure are the most attractive materials among various guided bone regeneration membranes. However, its osteogenic potential is still insufficient. This study was aimed to develop a Calcium surface-anchored Collagen I-PLGA/PCL scaffolds (PP/COL I-pDA-Ca) with enhanced osteogenicity. PP/COL I-pDA-Ca was electrospun from a collagen I-blended PLGA/PCL matrix and then modified by the chelation of Ca-ions via mussel-inspired polydopamine coating. PLGA/PCL, PLGA/PCL-polydopamine, PLGA/PCL-pDA chelated by Ca-ions were used as controls. Osteogenic effects of the scaffolds were examined using MC3T3-E1 cell culture. PP/COL I-pDA-Ca maintained 3D porous architecture with interconnected pores formed by randomly-oriented filamentous fibers and MC3T3-E1 cells cultured on it for 12 h or 24 h were more stretched and spread than those on the controls. PP/COL I-pDA-Ca significantly upregulated α10, α11 and β1 integrin expression after 48 h culture. ALP activity, OCN, OSX, BMP2 and RUNX2 expression of MC3T3-E1 cells cultured on PP/COL I-pDA-Ca scaffolds for 7 and 14 days were substantially enhanced when compared to controls ($p < 0.05$). The pDA-based Ca chelation, COL I incorporation and 3D bionic structure promoted cell adhesion and osteogenic differentiation of MC3T3-E1 cells. This novel PP/COL I-pDA-Ca scaffolds is an attractive alternative for guided bone regeneration.

1. Introduction

Recently, three-dimensional biodegradable synthetic scaffolds hold great promise for bone tissue engineering [1,2]. Bioactive materials have advantage of osteogenic (osteoconductive and osteoinductive)

* Corresponding author at: Center of Stomatology, the Second Affiliated Hospital of Soochow University, No. 1055 Sanxiang Road, Suzhou, Jiangsu Province 215004, China.
** Corresponding author.
E-mail addresses: guning@seu.edu.cn (N. Gu), yunzhu_qian@sina.com (Y. Qian).

https://doi.org/10.1016/j.matdes.2020.109300

properties and being immobilized onto biodegradable scaffolds to adjust osteogenic cell bioactivity for further bone regeneration in the target defect area [3–5]. The most-commonly used osteoconductive/osteoinductive materials are bioactive proteins (e.g. Collagen I, BMP2) [6–9], calcium phosphate ceramics e.g. β-tricalcium phosphate (β-TCP) and growth factors [10–13]. Inorganic ions, e.g. calcium (Ca), magnesium, silicon, strontium, have also been exploited as instructive ions for material-based bone tissue engineering strategies. Ca ions were reported to be successfully chelated onto the bio-scaffolds to improve bone cell activity. A blend of starch and poly caprolactone (SPCL) scaffolds were developed by a wet spinning technique with Ca and Si ions coagulation bath to enhance human adipose stem cells (hASCs) growth and induce osteogenic differentiation in the absence of osteogenic factors [14]. In addition, Ca and Si ions had a stronger influence on the osteogenic differentiation of hASCs in scaffolds than only Si ions.

Incorporation of inorganic ions into scaffolds traditionally focus on blending modification. However, the based-scaffolds may render uncontrolled and quick release of ions and weaken its effective effects. Mussel-inspired surface modification assisted by dopamine is acknowledged to be a promising and effective approach to immobilize inorganic constituents onto the surface of based-scaffolds [15,16]. Dopamine can modify various substrates by forming material-independent polydopamine (pDA) coating. The pDA ad-layer serves as a platform to deposit metal and bioceramics spontaneously as well as immobilize various adhesive proteins covalently [17,18]. Moreover, the pDA coating has no side effects on cells, and its further bioactive surface modifications on Poly (lactic-*co*-glycolic acid) (PLGA) electrospun scaffolds enhanced cell spreading and proliferation [19].

Bone is a composite material with an inorganic phase, hydroxyapatite and an organic phase, mainly composed of collagen. Inspired by biologically mimicking natural bone tissue, the ceramic-polymer composite scaffolds strategy e.g. a calcium-polymer based scaffold has been explored to repair bone defects by its high biocompatibility and osteoconductivity [20,21]. When the bio-scaffolds are delivered into the target bone defect area, it exhibits its capability including an intrinsic osteogenic activity and morphological features that are bone-comparable to reconstruct bone biologically. Local release of Ca ions from the bio-scaffolds can well sustain bone cell growth and satisfy new bone regeneration [22]. As a vital structure protein in ECM, collagen still has the capability to enhance the bio-affinity of nanofibers by being blended with synthetic polymers to make promising GTR/GBR scaffolds or modified onto the designed scaffold surface [23]. Hence, the combination of 3D porous mimic structure, collagen and Ca ions could provide an effective way to enhance the bone regeneration.

In normal physilological conditions, mature osteoblast populations produce the osteoid including collagen type I and calcium phosphate (apatite) mineral to form new bone [24].The PLGA and poly (caprolactone) (PCL) biodegradable composite could develop scaffolds with 3D porous structure by electrospinning. Under this inspiration, we fabricated a bionic scaffold with dual loads of Ca ions and collagen I via pDA coating and electrospinning to provide bone cells appropriate microenvironment composed of ECM-like 3D architecture and local delivery of Ca ions and collagen I. The prepared scaffolds would possess three vital elements: 1) Collagen I-PLGA/PCL was electrospun into a 3D ECM-like structure for bone cell growth. 2) Ca ions was chelated onto the surface of scaffold via polydopamine assisted surface modification for osteogenic promotion. 3) The scaffold was tailored to maintain mechanical supporting property and deliver Ca ions and collagen locally for synergistically osteogenic differentiation. We hypothesized that the Ca-chelated scaffolds would lead to good biocompatibility and double osteogenic effects from local release of Ca ions synergistically with COL I. To characterize the triple effect of Ca ions chelation, collagen I incorporation and 3D bionic PLGA/PCL electrospun architecture on osteogenic differentiation and assess its promising applications for guided bone regeneration, we performed physical, mechanical, biocompatible and osteogenic tests.

2. Experimental section

2.1. Synthesis of Ca^{2+}-chelated collagen I/ PLGA/PCL electrospun scaffolds

PLGA/PCL and Collagen I (2 wt%)/ PLGA/PCL 3D porous biodegradable electrospun scaffolds (PP and PP/COL I) were fabricated as previously described [25]: 0.7 g of PLGA (75:25, MW = 120,000) and 0.3 g of PCL (MW = 80,000) were dissolved in 7.3 g of 2,2,2-trifluoroethanol (TFEA; Aladdin, Shanghai, China), then 2 wt% Collagen I was added into PLGA/PCL solution. Two prepared blended solutions were stirred overnight for electrospinning.

To generate a polydopamine coated scaffolds, PP and PP/COL I scaffolds were submerged in 10 mM dopamine hydrochloride (AR, Sigma, USA) solution for 4 h. All the reaction system was processed in presence of oxygen [26]. The formed pDA-coated scaffolds were further dried under 40 °C for 24 h in a vacuum drying chamber. Ca ions was finally chelated onto pDA-modified samples by the one-step rapid reaction. The optimal concentration of $CaCl_2$ solution was investigated as 40 wt % and the most suitable reaction time was evaluated as 12 h, as shown in Fig. S1 (Supporting Information). So far, our novel PP/COL I-pDA-Ca and three controls: PP, PP-pDA, PP-pDA-Ca were ready. (Scheme. 1).

2.2. Physicochemical property testing

2.2.1. Structure, surface characterization and Ca ions release

A field emission scanning electron microscopy (FE-SEM; JSM-7401F, JEOL Ltd., Japan) was applied to characterize the surface topography and calculate fiber diameters for all scaffolds. An Energy Dispersive X-ray spectroscopy (EDS, Ultra Plus, Zeiss) was used to test sample elemental composition. The functional groups of the sample were measured by A Fourier Transform infrared spectroscopy (FTIR) spectrophotometer (Nicolet 6700). Water contact angles were determined by the contact angle meter (SL200B, Solon Technology Science, China) and the diameter of droplet was circa 0.2 mm. Each sample was tested six different positions. The results were statistically analyzed. PP-pDA-Ca and PP/COL I-pDA-Ca (2×2 cm^2) were soaked in 6 mL of phosphate buffered saline (PBS, pH = 7.4) at 37 °C. The solution was refreshed and collected at 1d, 4d, 7d, 10d, 13d and 15d. The concentration of Ca ions was measured by Inductively Coupled Plasma Mass Spectrometry (ICPMS, Thermo ICP-MS iCAPQ, ThermoFisher, USA).

2.2.2. Tensile property

All scaffolds were prepared into a 10 mm × 20 mm rectangular shape with an average thickness 0.15 mm for examining the tensile strength and elastic modulus using an electronic universal testing machine (INSTRON 3365, USA). Tightly clamped both ends by sand paper, each sample was tested at a 1 mm/min crosshead speed to obtain the yield point value of the stress-strain curve and the slope of the linear portion of the curve. The former was determined as the tensile strength and the later was as the elastic modulus.

2.3. In vitro cellular functions

The MC3T3-E1(MC) cell line subclone 14 (Cell Bank of the Chinese Science Academy, Shanghai, China). Cells were cultured and maintained as cell specification. Cells less than passage 10 were used for this study.

2.3.1. Live/dead cytotoxicity assay

The cytotoxicity of the scaffolds was investigated by cell live/dead staining (Calcein-AM/PI Double stain kit, YESEN, Shanghai, China). In brief, MC cells were cultured for 1 and 3 days on the four scaffolds, and collected by centrifugation at 1000 rpm for 5 min. The cells were stained with 2 μM calcein-AM (live cells, green fluorescence) and 4.5 μM PI (dead cells, red fluorescence) for 15 min at 37 °C away from light. Images were captured by Inverted fluorescence microscope (Olympus, IX73).

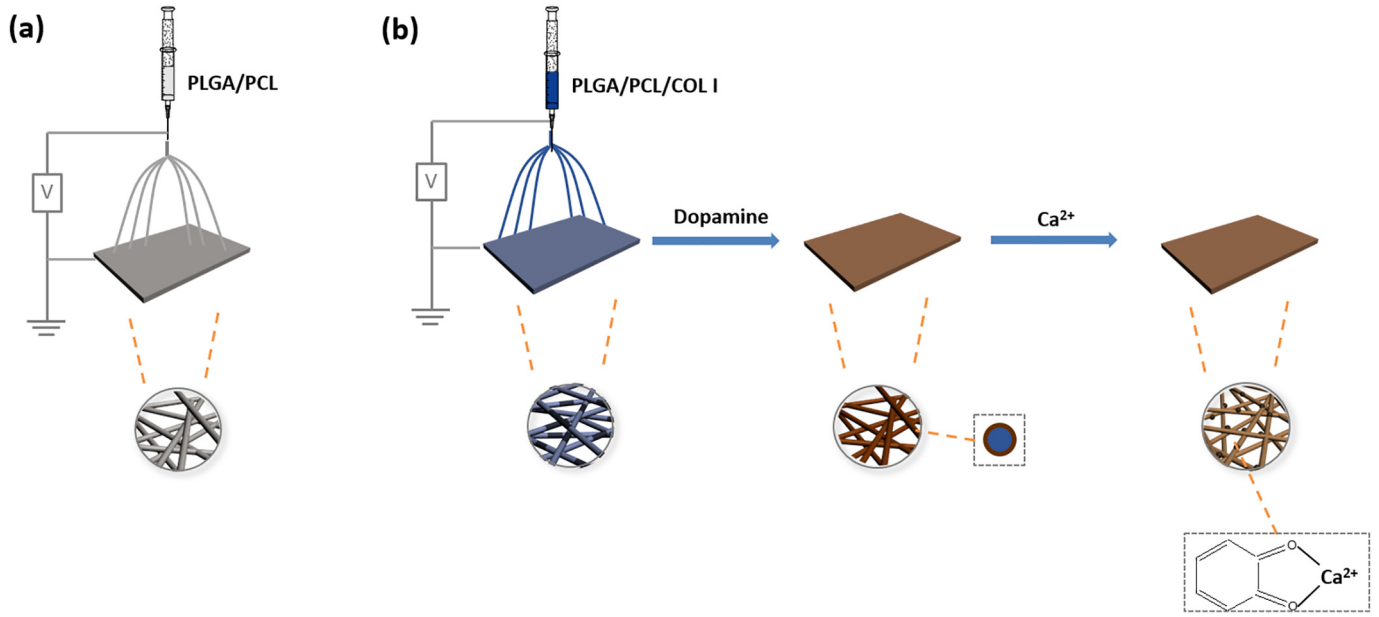

Scheme. 1. Illustration of the preparation procedure for PLGA/PCL scaffolds(a) and calcium surface-anchored Collagen I-PLGA/PCL scaffolds(b).

2.3.2. Cell proliferation

Cells (10^4/well) were seeded onto the 6 mm-diameter and 0.15 mm-mean thickness scaffolds in a 96-well plate in triplicate for 1, 3, 5 and 7 days of the culture. Cell Counting Kit-8 (CCK-8; Beyotime, China) were used to test cell viability and proliferation following the manufacturer's instruction. The optical density (OD) of formazan at 450 nm in the cell-on-scaffold groups was determined by an enzyme-linked immunosorbent assay plate reader (Titertek, Helsinki, Finland), compared with the scaffold-free cell control.

2.3.3. Cell morphology and cell adhesion

Cells (5×10^4 cells / well) were seeded onto the prepared 10 mm-diameter and 0.15 mm-average thickness scaffolds in a 24-well plate (5×10^4 cells / well) in triplicate for 24 h and 48 h of the culture. Surface topography and cell morphology of cell-on-scaffold groups was captured by FE-SEM and the Confocal Laser Scanning Microscopy (CLSM; Zeiss-LSM710; Carl Zeiss, Inc., Jena, Germany).

For cytoskeleton analysis, the samples were stained with rhodamine phalloidin (1:200 dilution; Cytoskeleton, Inc., Denver, CO, USA) after being fixed with 3.7% paraformaldehyde for 30 min at room temperature.

2.4. Integrin β1 immunofluorescence

Cell-on-scaffold groups were fixed after 24 h culture. Then all groups were incubated with anti-integrin β1 antibody (Abcam, ab52971) overnight. Further incubation was the secondary antibody (Alexa Fluor 488 goat anti-rabbit IgG, Beyotime, Shanghai, China) and rhodamine phalloidin for 15 min at room temperature for image capture by a Zeiss LSM 710 microscope. The CLSM image browser was used to analyze the images.

2.5. RNA isolation and RT-PCR

After the extraction of total RNAs by the TRIzol reagent (Invitrogen), the reverse transcription reactions were performed by the PrimeScript RT reagent kit (Clontech, Mountain View, CA). Real-time PCR reactions were prepared by the SYBR Premix Ex Taq kit (Clontech) using cDNA as the template. The sequences of primers used in this study are listed in Table 1. The real-time quantitative PCR for integrins, osteocalcin (OCN) and Osterix (OSX) genes was performed. The reaction in the ABI 7300 Real-time PCR System was: initial denaturation at 95 °C for 5 min; 40 cycles at 95 °C for 10 s, 60 °C for 31 s. The values of target gene expression were normalized to GAPDH and the relative gene expression values were calculated by the 2-ΔΔCt method.

Table 1
Primer Sequences of RT-PCR

Gene	Forward primer (5′-3′)	Reverse primer (5′-3′)
α1 Integrin	CTGCTGCCTGTGGACTTTAG	CTGGAGCGGTGGAAGAGTAA
α2 Integrin	GGGACCTCACAAACACCTTC	ACTGCTATGCCGAACCTCAG
α5 Integrin	GGGAGTGAGACCTGGCAACT	CTGGAGCGGTGGAAGAGTAA
α10 Integrin	TTGTGAGAGCAGCAAGGAAC	TAGTGACCAAGGACCGCAAT
α11 Integrin	AGGATGGGCTTGTGGACCTA	GACGGTTGCTGTTTGGAAGT
β1 Integrin	ATCCCAATTGTAGCAGGCGTGGTT	GACCACAGTTGTCACGGCACTC
OCN	TCGTGTGTCTTCTCCACAGC	TGGCCACTTACCCAAGGTAG
OSX	CCCCTGTTCTTCACAGCTTC	GGGAAAACGGCAAATAGGAT
GAPDH	CCTTCCGTGTTCCTACCC	CAACCTGGTCCTCAGTGTAG

OCN- osteonectin, OSX – ostrix.

2.6. Alkaline phosphatase (ALP) assays

After 7d and 14d cell-on-scaffold culture, cells were collected by centrifuging at 1000 rpm for 5 min from the scaffolds and lysed with RIPA buffer. Cell lysates were homogenized and centrifuged to remove insoluble material at full speed for 3 min, and the supernatants were collected for ALP testing. The ALP activity was determined using the Alkaline Phosphatase Assay kit (Beyotime), and the OD values were measured via a microplate reader (Multiskan MK3, Thermo Scientific, Shanghai) at 405 nm. ALP activity was normalized to the total protein content.

2.7. Western blot

Total protein was extracted from the collected cells with RIPA buffer containing 1% PMSF. Then the protein concentration was assessed by the Bradford method. Anti-BMP2 antibody (ab14933, Abcam; 1:500 dilution), anti-*Runx2* antibody (ab23981, Abcam; 1:1000 dilution) and anti-rabbit IgG (ab6721, Abcam; 1:2000 dilution) were used in the western blot analysis. GAPDH was as the internal control. The enhanced chemiluminescence reagent (Thermoscientific, Rockford , IL, USA) was used to detect immunoreactive bands. The results were analyzed by the ImageJ (NIH, Bethesda, USA) and GraphPad Prime 5.0 software.

2.8. In vivo implantation

Based on the cytotoxic test results and following the 3R rules (replacement, reduction and refinement) of animal experiments, all four scaffolds (measuring 5×5 mm^2, $n = 5$) were prepared and implanted into the back of the mice below the subcutis. After two-week implantation, the mice were sacrificed and the implants were dissected and processed for hematoxylin and eosin (H&E) staining. In brief, deparaffinized and rehydrated sections were dipped in hematoxylin for 3 min and in eosin for 1 min, then dehydrated in an ascending ethanol series and cleared in xylene. Then histological appearance of four implants were captured. Experiments were carried out in accord with protocols that were approved and monitored by the Institutional Animal Care and Use Committee at Soochow University (Approval No. ECSU-201800078) and the Association of laboratory animals in Jiangsu Province, China.

2.9. Statistical analysis

Data were analyzed in SPSS ver22 (SPSS, Chicago, IL, U.S.A.) and all experimental data were shown as mean ± standard deviation (Mean ± SD). After testing the normality, statistical analysis was performed at $p = 0.05$ using one-way analysis of variance and the least significant difference test. All quantitative data were averaged at least three independent experiments.

3. Results and discussion

3.1. Surface topography of the PP/COL I-pDA-Ca and control scaffolds

SEM analysis demonstrated that all four scaffolds featured unique porous morphology to electrospinning that was not seen in nanostructure produced by other techniques. (Fig. 1 Aa-Dd) The fiber mats of the four scaffolds had a random and nonwoven structure. It exhibited a 3D porous network with interconnected pores formed by randomly-oriented filamentous electrospun fibers.

The mean nanofiber diameter in the PP was 426 ± 137 nm, and the fiber surfaces were relatively rough following pDA coating and Ca ions immobilization. However, PP-pDA and PP-pDA-Ca maintained the 3D porous structure with similar fiber diameter to the PP. The average pore size of PP-pDA and PP-pDA-Ca was about 2 μm. The average fiber diameter of the PP/COL I-pDA-Ca was about 417 ± 150 nm, thinner than that of PP, PP-pDA, PP-pDA-Ca. It was attributed to the incorporation of COL I into PP solution that lowered the viscosity of the electrospinning solution. The average pore size of PP/COL I-pDA-Ca was about 1.8 μm. The successful chelation of Ca ions on the PP-pDA-Ca and PP/COL I-pDA-Ca was confirmed by EDX analysis in Fig. 1 E. Ca element were distributed uniformly on two scaffolds by the chelation of polydopamine, as showed in Fig. S2 (Supporting Information).

Electrospun scaffolds can provide larger specific surface area and more bioactive sites to bind functional materials and further enhance cell adhesion [27]. In this study, all the synthetic scaffolds demonstrated great performance of 3D architecture even undergoing these modifications. It possessed structural integrity to prevent pores from collapsing that would benefit cell attachment, proliferation and penetration [28].

3.2. Physicochemical properties of the PP/COL I-pDA-Ca and control scaffolds

The FTIR spectra of the PP, PP-pDA, PP-pDA-Ca, and PP/COL I-pDA-Ca was shown in Fig. 2A. It found typical absorption peaks in all the PLGA/PCL scaffolds at about 1757 cm^{-1} and 1727 cm^{-1}, assigned to the free ester functional group (-COOR) in PLGA [29]and the conjugated ester groups (-OCOR) in PCL [30], respectively. In the PP-pDA, the -C=O stretching vibration peaks were observed at 1186 cm^{-1} and 1092 cm^{-1} [31]. There

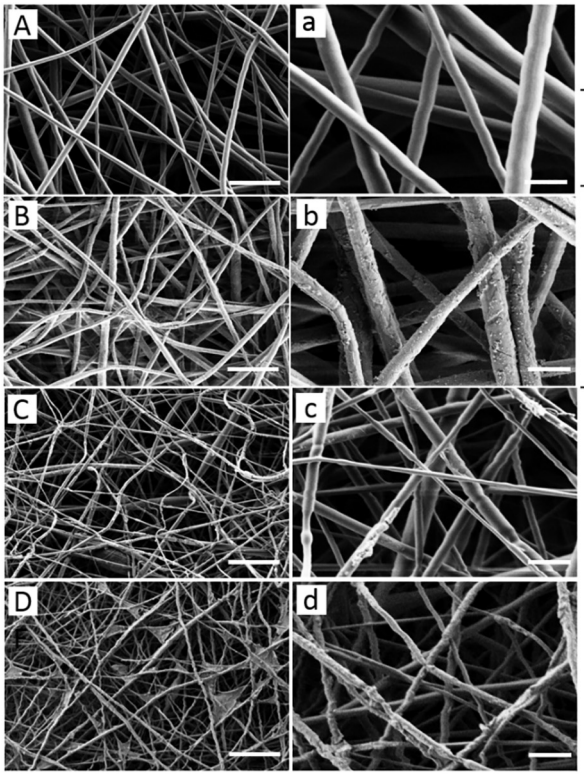

E

Sample	Atomic composition (%)		
	C	O	Ca
PP	63.58	36.42	0
PP-pDA	64.85	35.15	0
PP-pDA-Ca	62.29	37.63	0.08
PP/COL I-pDA-Ca	61.05	38.88	0.07

Fig. 1. Structure and composition of the PP/COL I-pDA-Ca and control scaffolds. FE-SEM images of the PP (A, a), PP-pDA (B, b), PP-pDA-Ca (C, c) and PP/COL I-pDA-Ca (D, d) scaffolds at lower (A, B, C and D, scale bar is 10 μm) and higher (a, b, c and d scale bar is 2 μm) magnification. Note that all four scaffolds exhibited unique 3D architectures which were composed of randomly-oriented nanofibers and mimicked the arrangement of native extracellular matrices. (E). Elemental composition of the scaffold surfaces. C-Carbon, O-Oxygen, Ca-Calcium.

were obvious absorption peaks at 1240 cm^{-1}, 961 cm^{-1} assigned to the -NH and -OH stretching vibration in pDA, indicating the successful modification of pDA coating on PP [32]. There was almost no variation of PP-pDA-Ca as compared to PP-pDA. The observed peaks at 1652 cm^{-1} and 1550 cm^{-1}, Which correspond to C═O stretching vibration and N—H vibration respectively, were appeared in PP/COL I-pDA-Ca. A broad peak at 3325 cm^{-1} were the representative indication of -OH and -NHCO in COL I, confirming the successful incorporation of COL I into PP scaffolds [33].

Mechanical strength of the biodegraded nanofiber scaffolds is vital to mimic natural structure e.g. extracellular matrix (ECM). As shown in Fig. 2B, the mean Young's modulus values of the PP, PP-pDA, PP-pDA-Ca and PP/COL I-pDA-Ca were 40.78 ± 4.62, 36.89 ± 3.91, 29.53 ± 5.20, and 28.53 ± 2.02 MPa while the fracture stress values of the PP, PP-pDA, PP-pDA-Ca and PP/COL I-pDA-Ca were 2.82 ± 0.004, 2.13 ± 0.005, 2.42 ± 0.007, 2.69 ± 0.003 MPa, respectively. The common tensile strength of cancellous bone in elasticity modulus ranges from 1 to 20 MPa and the Fracture stress varies from 0.05 to 0.5 GPa [34]. The mechanical properties of the PP/COL I-pDA-Ca were similar to the electrospun PLGA/PCL membranes fabricated by Chou and et al. [35], indicating that PP/COL I-pDA-Ca can well support cells growth in bone defect area. The chelation of Ca ions resulted into the decrease of Young's modulus values. Some functional groups (such as phenolic hydroxyl groups) of polydopamine were acted with Ca ions [36]. Therefore, the elastic modulus of external polydopamine layer declined.

The wettability on the surfaces of the scaffolds was measured by Water Contact Angle (Fig. 2C). The water contact angles of PP, PP-pDA, PP-pDA-Ca and PP/COL I-pDA-Ca are about 121.9 ± 1.0°, 81.8 ± 3.7°, 104.6 ± 2.5°, and 98.7° ± 4.4°, respectively. The PP-pDA surface was more hydrophilic owning to pDA coating than PP [37].However, further Ca chelation by pDA coating rendered the PP-pDA-Ca less hydrophilic than PP-pDA, indicating that the deposited Ca on the surface of scaffolds resulted in the loss of hydrophilic groups. Incorporation of Collagen I in PP and then Ca chelation by pDA coating, the water contact angle of the PP/COL I-pDA-Ca dropped to 98.7° ± 4.4°. These results demonstrated that PP/COL I-pDA-Ca increased its hydrophilic properties owing to the pDA coating and Collagen I and can provide a better physiological environment for cell growth [38].

The release of Ca ions from PP-pDA-Ca and PP/COL I-pDA-Ca in PBS (pH = 7.4) was shown in Fig. 2D. The release rate of both samples was quick within 7 days and then decreased gradually. The cumulative release amount of Ca ions from PP-pDA-Ca and PP/COL I-pDA-Ca were 2.83 and 2.01 μg/cm^2 within 15 days, respectively. The release curve would rely on the interaction between polydopamine and Ca ions and the results showed that the incorporation of COL I decreased the release amount of Ca ions.

3.3. The effects of the scaffolds on MC3T3-E1 cellular functions

3.3.1. Cell cytotoxicity and proliferation

To determine the effect of our scaffolds on cell proliferation, all four scaffolds were seeded with MC3T3-E1 cells, and their proliferative capability was evaluated based on CCK-8 assays. As shown in Fig. 3, MC3T3-E1 cells had highest proliferation rate on PP/COL I-pDA-Ca at 3d, indicating that COL I incorporation and pDA coating-assisted Ca chelation can

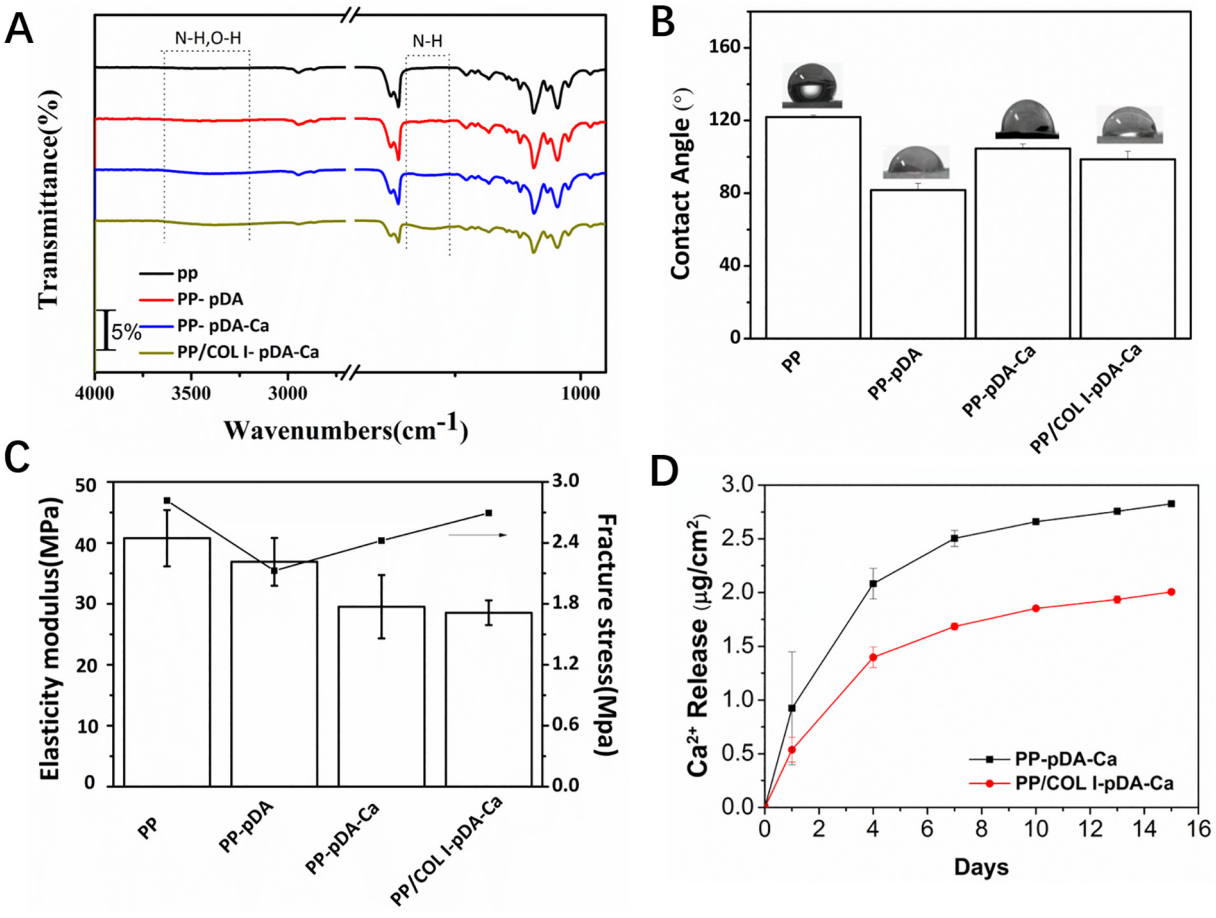

Fig. 2. Physicochemical and mechanical properties of the PP/COL I-pDA-Ca and control scaffolds PP, PP-pDA, PP-pDA-Ca. (A). FTIR spectra. (B). Mechanical properties of tensile strength and elastic modulus. The elastic modulus (left Y axis) is compared among the four scaffolds by column chart while the tensile strength (right Y axis) is compared by the line chart. Note that PP/COL I-pDA-Ca maintained the elastic modulus and fracture stress with the incorporation of type I collagen and Ca chelation by pDA coating. (C). Contact angle. The images above each column illustrate the actual contact angle when water drops onto the scaffolds. (D). The release behavior of Ca ions from Ca-chelated scaffolds.

increase the affinity of the scaffolds to the cells [39]. The composite scaffolds are expected to display better biological activity and improved cell response via changes in surface topography and chemistry on degradable polymer scaffolds by collagen incorporation and Ca coating [40,41]. At 5d and 7d, cells proliferated well on all four scaffolds although no significant difference in cell proliferation rate was found among groups, signifying that our base scaffold and subsequent modifications were non-toxic. This were further confirmed by the results of live/dead staining of MC3T3-E1 on the four scaffolds (Fig. 4). Dead cells were rarely found in fluorescent microscopy images. The number of live cells was the largest on the PP/COL I-pDA-Ca at 7d, indicating that PP/COL I-pDA-Ca can improve cell proliferation via COL I incorporation and pDA coating-assisted Ca chelation.

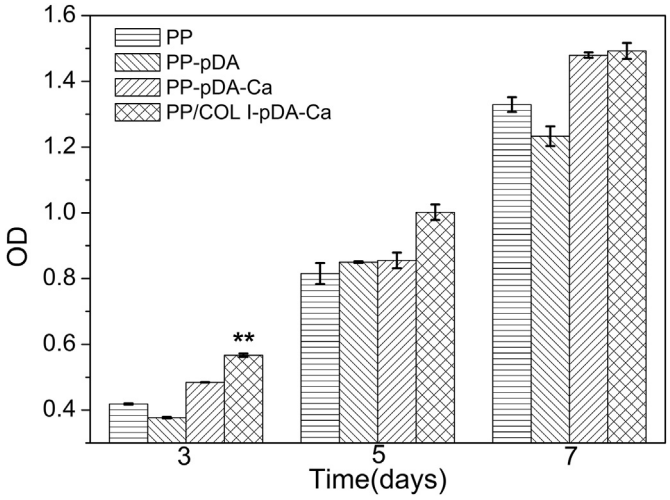

Fig. 3. The CCK-8 assay of PP, PP-pDA, PP-pDA-Ca and PP/COL I-pDA-Ca scaffolds. MC3T3 cells were seeded onto the four scaffolds and cultured for 3, 5 and 7 days. * $p < 0.05$, ** $p < 0.01$, compare with PP.

3.3.2. Cell morphology and attachment

We used FESEM and CLSM to capture the images that how our PP/COL I-pDA-Ca and control scaffolds affected cell morphology and the interaction between MC3T3-E1 cells and their environment, including cell attachment and spreading. As illustrated in Fig.5A, MC3T3-E1 cells spread along the randomly-oriented nanofibers, extended filopodia in the same directions as the nanofiber orientations and penetrated into the 3D-porous structure of all four scaffolds, indicative of the well-designed structure of these 3D electrospun scaffolds for cell inhabitation and their ability to create a favorable microenvironment for cell recruitment. There were more cells attached on the PP/COL I-pDA-Ca when compared to the other scaffolds. Moreover, the cellular pseudopods attached on the scaffolds have crossed each other and form a cell layer on the surface, suggesting that PP/COL I-pDA-Ca enhanced MC3T3-E1 cells attachment and spreading.

CLSM images provided evidence how the effect of our scaffolds on MC3T3-E1 cell cytoskeletal morphology. As shown in Fig. 5B, the 3D distribution of MC3T3-E1 cells, cell attachment and scaffold infiltration for all four electrospun scaffolds were displayed. Well-shaped actin fibers and extended filopodia along the invisible randomly-oriented nanofibers that were spread in 3D in multiple directions. The number of cells attaching onto the four scaffolds after 12 h culture was 24 ± 1/field (PP/COL I-pDA-Ca), 23 ± 1/field (PP-pDA-Ca), 10 ± 0/field (PP-pDA), 8 ± 1/field (PP), respectively. Statistic differences were significant between groups after 12 h culture (all $p < 0.05$). The number of cells attaching onto the four scaffolds after 24 h culture was 29 ± 2/field (PP/COL I-pDA-Ca), 26 ± 1/field (PP-pDA-Ca), 26 ± 2/field (PP-pDA), 24 ± 1/field (PP), respectively. PP/COL I-pDA-Ca was significantly different with PP-pDA-Ca, PP-pDA and PP after 24 h culture (all $p < 0.05$), but no significant difference was found between three control

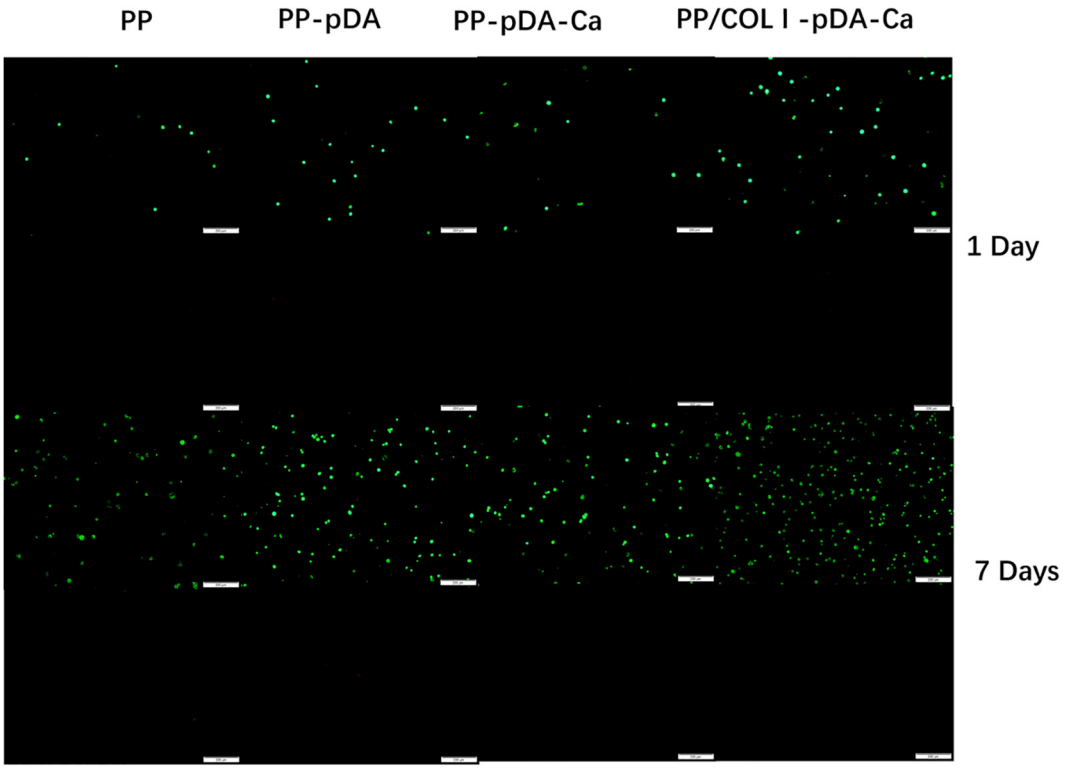

Fig. 4. The Live- Dead cell assay of PP, PP-pDA, PP-pDA-Ca and PP/COL I-pDA-Ca scaffolds at 1 day and 7 days. Live cells stained green, dead cells stained red.

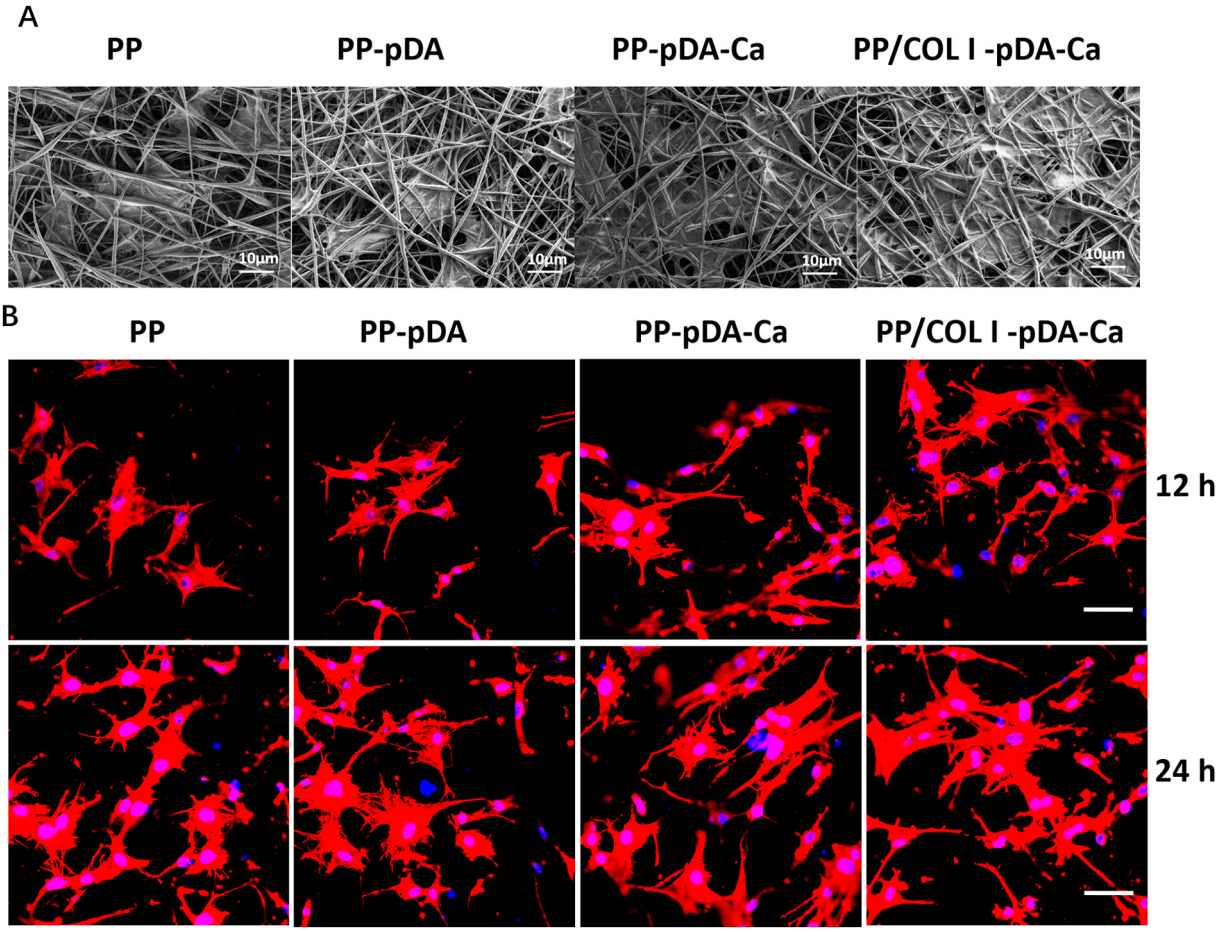

Fig. 5. Cell morphology and attachment on the PP/COL I-pDA-Ca and control scaffolds. MC3T3-E1 cells were cultured on the PP, PP-pDA, PP-pDA-Ca, and PP/COL I-pDA-Ca scaffolds for 12 h or 24 h. (A) FESEM images of the scaffolds with cultured cells for 24 h. (B) Fluorescent staining of cytoskeleton after the cells were cultured for 12 h and 24 h. Note that the MC3T3-E1 cells on the PP/COL I-pDA-Ca had higher cell density and were well spread.

groups after 24 h culture. After 12 h, MC3T3-E1 cells cultured on the PP-pDA, PP-pDA-Ca spread slightly better than on the PP, and MC3T3-E1 cells exhibited the widest range of spreading on our PP/COL I-pDA-Ca. After 24 h culture, cell spreading was improved on all scaffolds compared to cell spreading after 12 h culture (Fig. 5B). After 12 h and 24 h culture, the actin cytoskeleton of MC3T3-E1 cells attached to PP/COL I-pDA-Ca spread and stretched further than cells on the other three scaffolds. This finding was consistent with our SEM results, further confirming that PP/COL I-pDA-Ca promoted cell attachment and spreading.

3.3.3. The effects of the scaffolds on integrin expression in MC3T3-E1 cells

Integrins regulate cytoskeletal dynamics, thereby influencing a number of crucial cellular processes, for example, cell adhesion, migration and differentiation [42]. It is well known as a family of heterodimeric transmembrane receptors consisting of an α and a β subunit, which can specifically bind to the specific binding sites like RGD or DGEA sequence within the ECM protein as well as Ca^{2+} binding area [43,44].

Integrins α1, α2, α5, α10, α11 and β1 participate in cell adhesion and cell-surface mediated signaling. α1, α2, α10 and α11 are I-domain collagen-binding subunits that play a central role in ligand binding and intercellular adhesion [43], and the α1β1, α2β1, α10β1 and α11β1 integrins serve as receptors for collagens [44] and are known to mediate adhesion to collagen type I and/or type II. In detail, α1β1 is the preferential receptor for collagen type VI and α2β1 is the preferential receptor for collagen type II [45]. α5β1 is the fibronectin receptor [46]. α11β1 is the preferential receptor for collagen type I [47]. α10β1 interacts with collagen type II and is closely related to the other collagen-binding integrins α1β1, α2β1 and α11β1. α1β1 and α2β1 are also known to mediate adhesion to laminin [48].

In the present study, MC3T3-E1 cells were cultured on the PP/COL I-pDA-Ca and control scaffolds for 12, 24 and 48 h, and the expression of α1, α2, α5, α10, α11 and β1 integrin was examined using real time RT-PCR analysis (Fig. 6). Statistic differences were significant between groups ($p < 0.001$, except $p = 0.002$ in α2 between PP-pDA and PP/COL I-pDA-Ca after 48 h cell culture). After 12 h of culture, the expression of all six integrins was significantly upregulated in the PP-pDA-Ca and PP/COL I-pDA-Ca groups compared to the PP group ($p < 0.001$). The expression levels of integrinα1, α2, α10, α11 and β1 were generally higher than that of α5 at three time points (Fig. 6). PP/COL I-pDA-Ca had highest expression levels of α1, α2, α11and β1 while PP-pDA-Ca had highest expression levels of α10. After 24 h culture, PP/COL I-pDA-Ca had highest expression levels of α1, α10 while PP-pDA-Ca had highest expression levels of β1. After 48 h of culture, PP/COL I-pDA-Ca had highest expression levels of α10, α11 and β1 while PP-pDA-Ca had highest expression levels of α1, α2 and α5. Upregulation of integrin β1 expression at the protein level in MC3T3-E1 cells cultured on PP/COL I-pDA-Ca and control scaffolds was further confirmed using immunofluorescence (Fig. 7). Confocal microscopy images demonstrated all three modified scaffolds by pDA coating enhanced integrin β1 expression. Notedly, PP/COL I-pDA-Ca promoted highest β1 integrin expression levels in MC3T3-E1 cells after 24 h culture on the scaffold when compared to the control scaffolds.

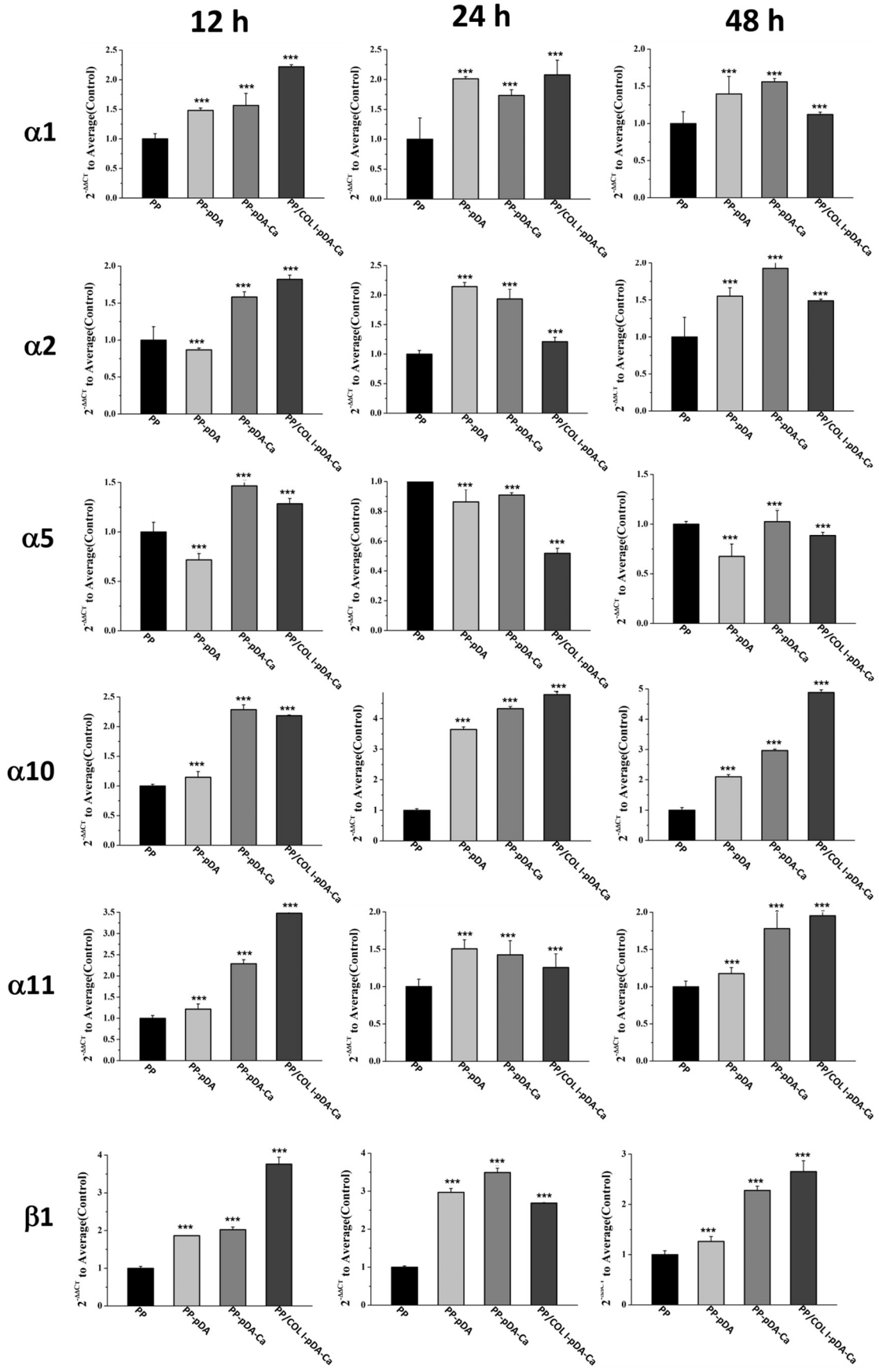

Fig. 6. Integrins β1, α1, 2, 5, 10, 11 expression in MC3T3-E1 cells cultured on PP, PP-pDA, PP-pDA-Ca and PP/COL I-pDA-Ca scaffolds. MC3T3-E1 cells were cultured on the scaffolds for 12 h, 24 h and 48 h. The expression of target genes was normalized to GAPDH and the relative expression level was calculated by the $2^{-\Delta\Delta Ct}$ method. *** $p < 0.001$, compare with PP.

Surface topography and chemical composition both have influence on the interaction between cell and the substrates, and on protein adsorption, integrin expression, and cell behavior. It has been reported that scaffolds or other substrates coated with ECM proteins like collagen I or fibronectin have greatest capacity to increase integrin expression, and thus osteoblast adhesion, proliferation and differentiation [44]. The incorporation of COL I into the polymer scaffolds can enhance osteogenic cell adhesion to the surface of the scaffolds by increasing integrin expression [19]. Polydopamine coating was reported to exert direct enhancing on the cell adhesion, proliferation, and differentiation of osteoblasts [49] and osteogenic differentiation of bone marrow derived mesenchymal stromal cells on pDA-coated substrate by integrin-mediated cell-matrix adhesion mechanisms [50,51]. Here we have demonstrated that pDA coating on the PP scaffold surface increased the expression of collagen receptors $\alpha1\beta1$, $\alpha2\beta1$, $\alpha10\beta1$ and $\alpha11\beta1$, indicating that pDA-coated PP scaffolds promoted the interactions between MC3T3-E1 cells and collagens. Ca chelation via pDA coating onto the PP had significantly higher expression of collagen receptors $\alpha1\beta1$, $\alpha2\beta1$, $\alpha10\beta1$ and $\alpha11\beta1$ compared with PP and PP-pDA, signifying that Ca ions collaborated with pDA coating and further increased the interactions between MC3T3-E1 cells and collagens. Probably $\alpha10\beta1$ closely related to the other collagen-binding integrins $\alpha1\beta1$, $\alpha2\beta1$ and $\alpha11\beta1$. And the differences found in attachment and adhesion of integrin mediated cell response to the implant material can be differences in substrate composition and topography, availability of proteins in the culture medium and accessibility of the binding sites [44]. The variation of integrin upregulation between PP/COL I-pDA-Ca and PP-pDA-Ca from 12 h to 48 h might be explained mainly by the incorporation of collagen type I resulting in the change of chemical composition, the subsequent change of surface topography by Ca ions chelation via pDA-coating and the competition of Ca ions and collagen type I to the collagen-binding integrins. Although incorporation of collagen type I into the scaffold combined with pDA-assisted Ca chelation resulted in higher $\alpha10$, $\alpha11$ and $\beta1$ integrin expression levels at 48 h, Ca ions seemed to preferentially compete the $\alpha1$, $\alpha2$ binding sites with collagen type I. Overall, PP/COL I-pDA-Ca scaffold promoted MC3T3-E1 cell adhesion and Ca ions probably preferred to binding to integrin $\alpha1$, $\alpha2$ and collaborated with collagen I to promote cell adhesion.

3.3.4. Cell differentiation

3.3.4.1. ALP, OCN and OSX analysis. ALP activity is intended to evaluate the early differentiation and mineralization. In this study, the ALP activity of MC3T3-E1 cells cultured on four scaffolds for 7 and 14 days was evaluated. As shown in the Fig. 8, the results revealed that the ALP activity of MC3T3-E1 cells cultured on PP/COL I-pDA-Ca increased over time and was significantly higher when compared to MC3T3-E1 cells cultured on three controls ($p < 0.05$), indicating that the modified scaffolds enhanced osteogenic differentiation of MC3T3-E1 cells. The synergistic effect of pDA-coated Ca chelation and COL I incorporation for the 3D PLGA/PCL scaffolds was more effective than the single pDA-coated Ca chelation to up-regulated osteoblast differentiation.

The osteo-differentiation of MC3T3-E1 cells was measured by the expression of OCN and OSX genes by RT-PCR (Fig.9). OCN is the most important bone biomarkers responsible for initiation and maintenance of bone mineralization [52]. Osterix is downstream gene of Runx2, and a transcription factor that is indispensable for osteoblast differentiation [53]. The expression of OCN and OSX in the PP/COL I-pDA-Ca and PP-pDA-Ca groups were higher than the PP group. More importantly, OCN and OSX in the PP/COL I-pDA-Ca group were significantly upregulated on day 14, indicating that PP/COL I-pDA-Ca had good osteogenic capacity to enhance cell differentiation and mineralization.

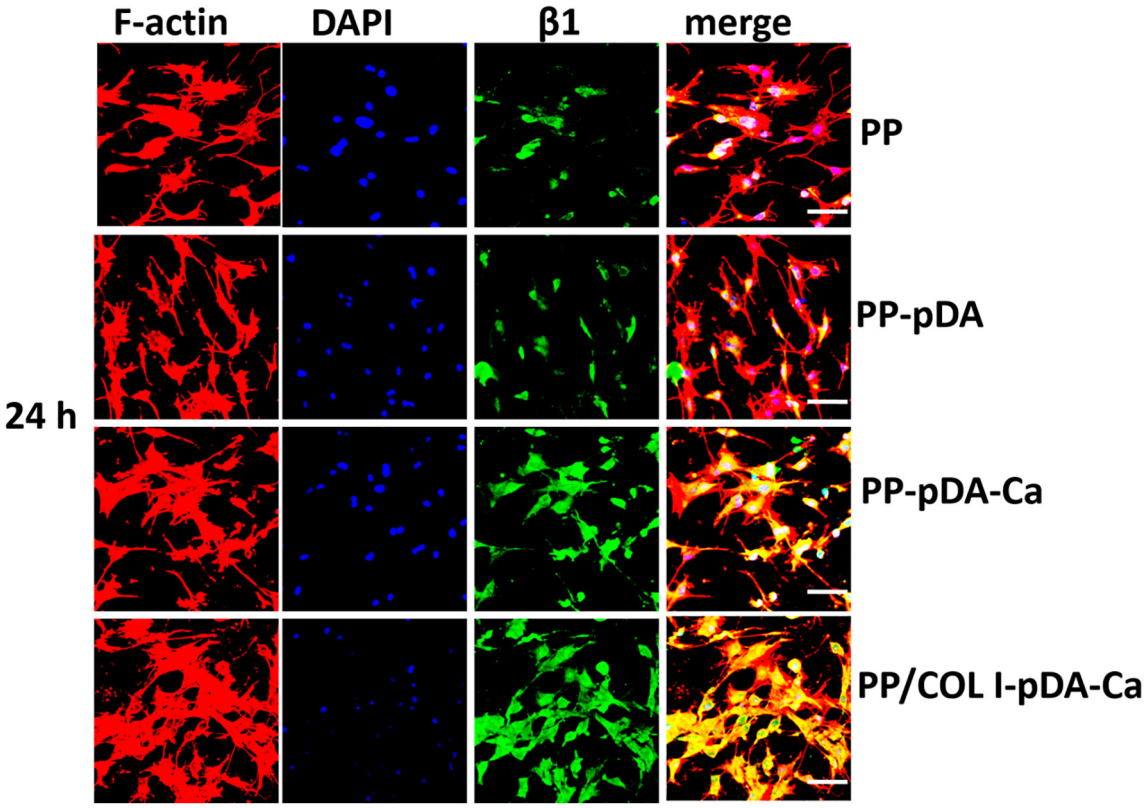

Fig. 7. Integrin $\beta1$ expression in MC3T3-E1 cells cultured on PP/COL I-pDA-Ca and control scaffolds. MC3T3-E1 cells were cultured on the scaffolds for 24 h and then fluorescently labeled for F-actin (red) or for integrin $\beta1$ via immunofluorescence (green). Note the increased levels of integrin $\beta1$ on the MC3T3-E1 cells on the PP/COL I-pDA-Ca.

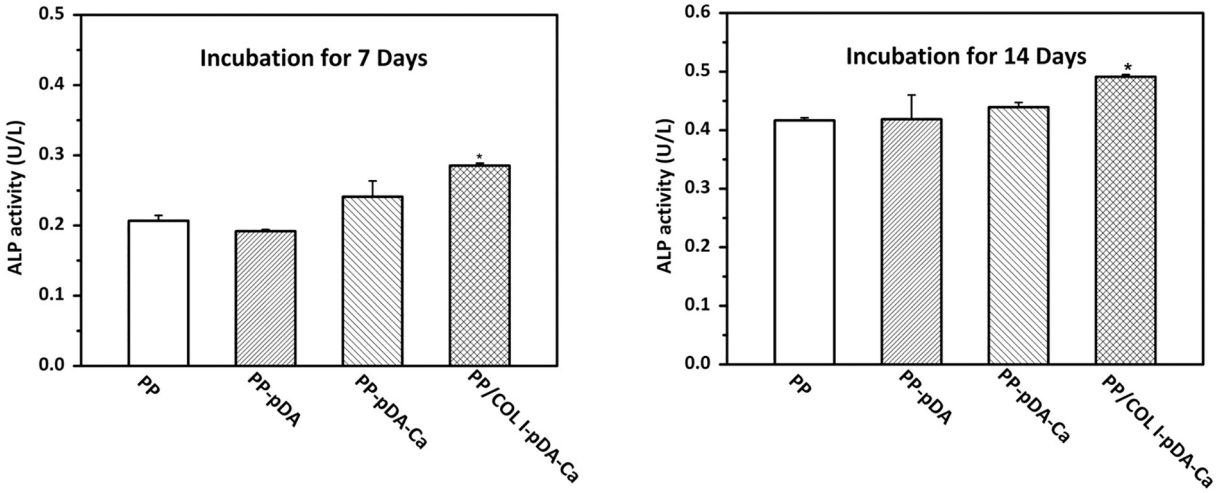

Fig. 8. Effects of the PP/COL I-pDA-Ca and control scaffolds on osteogenic differentiation of MC3T3-E1 cells was evaluated by ALP activity. Cells were cultured on the scaffolds for 7 or 14 days. ALP activity was determined using an alkaline phosphatase assay kit and normalized to the total protein content. * $p < 0.05$ compare with PP.

3.3.4.2. Western blot analysis. The osteogenic differentiation of MC3T3-E1 cells is regulated by BMP2 and RunX2 [54]. Western blot analysis revealed that BMP2 and RUNX2 expression levels were significantly upregulated in MC3T3-E1 cultured on PP-pDA, PP-pDA-Ca and PP/COL I-pDA-Ca at day 7 and day 14, compared to PP as shown in Fig. 10. The effect on BMP2 and RUNX2 expression levels was in the order of

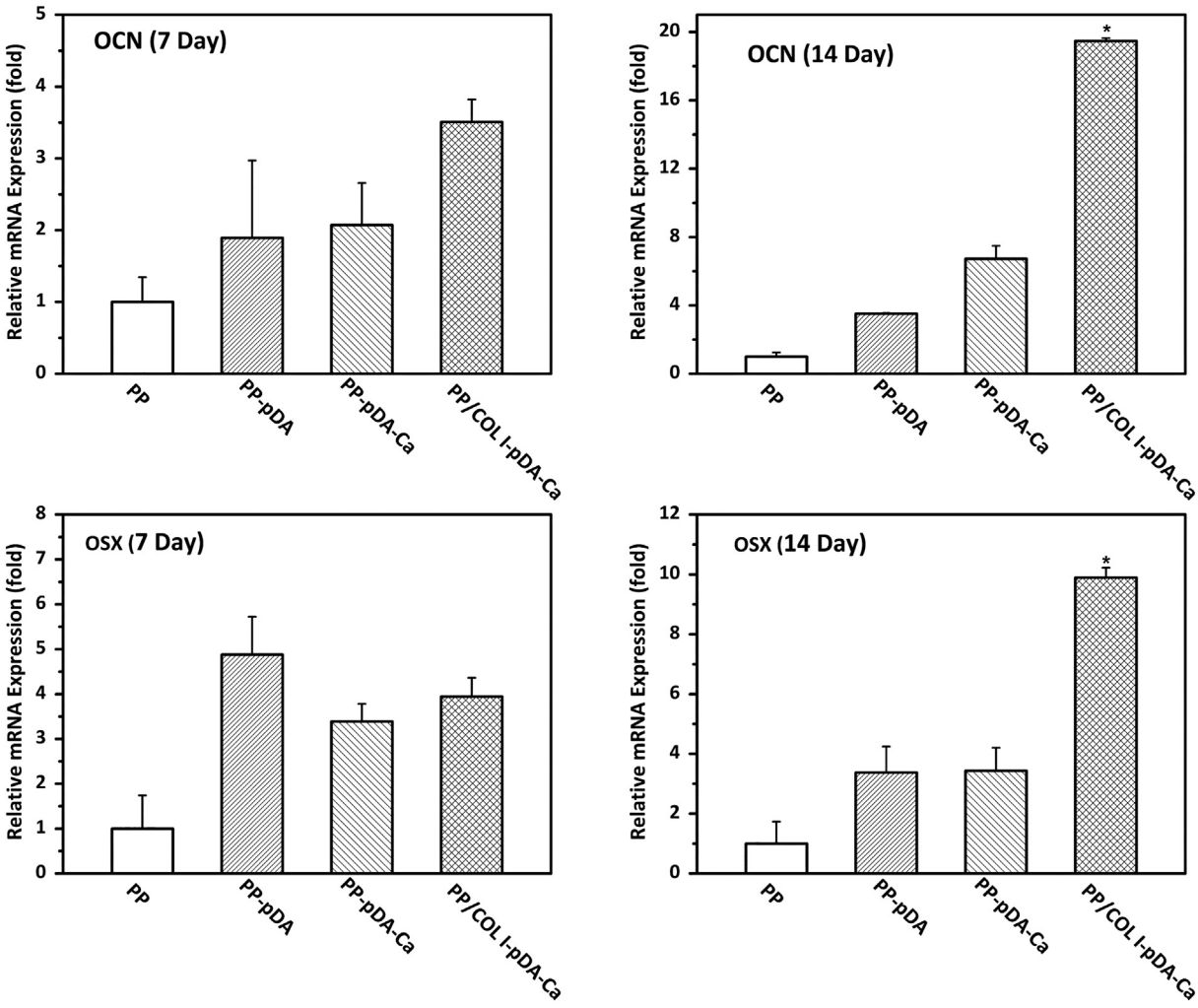

Fig. 9. OCN, OSX mRNA expression of MC3T3-E1 cells cultured on on the PP, PP-pDA, PP-pDA-Ca, and PP/COL I-pDA-Ca scaffolds for 7 days and 14 days. The expression of target genes was normalized to GAPDH and the relative expression level was calculated by the $2^{-\Delta\Delta Ct}$ method. * $p < 0.05$, compare with PP.

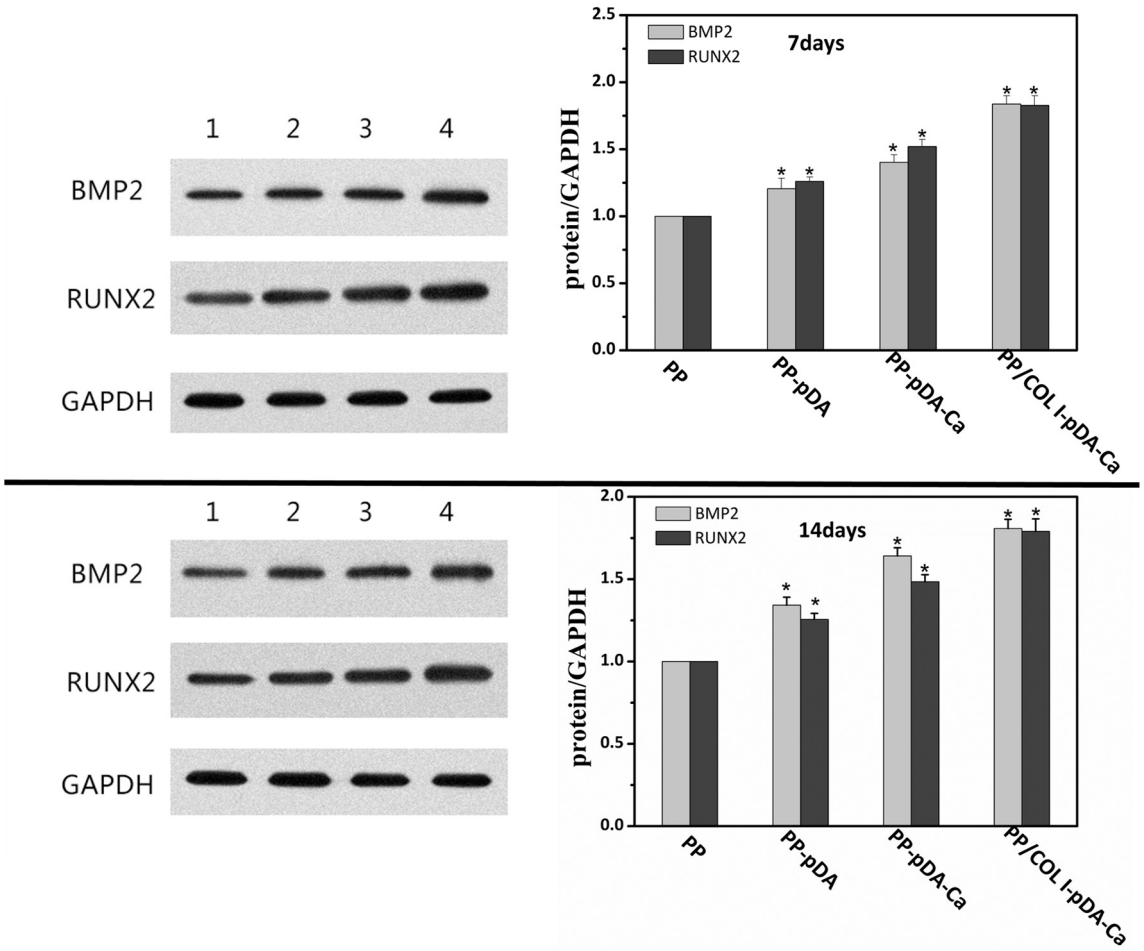

Fig. 10. The protein expression of BMP2 and RUNX2 when MC3T3-E1 cells were cultured on the PP/COL I-pDA-Ca and control scaffolds for 7 and 14 days was determined by Western blotting. The expression levels were calculated by densitometry analysis relative to GAPDH. * $p < 0.05$ compare with PP.

PP < PP-pDA < PP-pDA-Ca < PP/COL I-pDA-Ca ($p < 0.05$), suggesting that surface modifications on PLGA/PCL scaffold by pDA-coated Ca chelation and collagen I blending into basic matrix enhanced MC3T3-E1 cell differentiation. PP/COL I-pDA-Ca displayed the highest expression levels of BMP2 and RUNX2, probably owing to the synergistic effects of immobilizing Ca ions by pDA-coating onto PLGA/PCL electrospun scaffolds with collagen I incorporation.

In recent years, collagen I has been widely investigated and exhibits excellent properties that facilitate cell attachment as well as enhance surface bioactivity by modifying biomaterial surfaces [19]. Collagen blending PCL or PLGA electrospun scaffolds have been shown to support cell adhesion, assist cell infiltration, enhance cell proliferation, stimulate cell growth and differentiation in vitro, induce vascular formation, and maintain structural integrity in vivo [55]. In osteogenic differentiation and mineralization of preosteoblasts, collagen synthesis precedes the expression of osteogenic markers indicating that the interaction of ECM components with the integrin family of cell surface receptors plays a role in the induction of osteogenesis [56,57]. PDA-coated calcium bio-inspired modifications were found to enhance cell adhesion with higher expressions of cell adhesion markers, promote cell attachments and proliferation with higher secretion of ECM proteins, such as collagen I and fibronectin, improve cell differentiation with increased ALP activity and osteogenesis-related proteins [58]. Our results demonstrated that immobilized Calcium by pDA-coating onto PLGA/PCL electrospun scaffolds with collagen I incorporation synergistically promoted MC3T3-E1 cell adhesion, proliferation and osteogenic differentiation, matching earlier studies.

3.4. In vivo effect of the scaffolds on stem cell recruitment

The in vivo application of PP/COL I-pDA-Ca and control scaffolds for stem cell recruitment and growth was investigated by subcutaneous implantation. The numbers of cell penetrating into four scaffolds were 295 ± 45/field (PP/COL I-pDA-Ca), 91 ± 19/field (PP-pDA-Ca), 53 ± 5/field (PP-pDA), 28 ± 8/field (PP), respectively. PP/COL I-pDA-Ca had significantly more cell infiltration than three control scaffolds. The cell infiltration number of PP-pDA-Ca was also significantly different from the other three scaffolds while no significant difference was found in the cell infiltration number between groups of PP and PP-pDA, indicating that Ca ions chelation onto the PLGA/PCL scaffolds via pDA-coating as well as the blending of collagen I into the PLGA/PCL matrix enhanced the cell response to the prepared scaffolds and the synergistic functionality of PP/COL I-pDA-Ca was prominently increased and about 10-fold to the basic PP scaffold (Fig. 11).

As reported, the introduction of calcium into the polymer component or polymer blends for biomedical materials affected the mechanical properties of the resulting hybrids either by chelation [59], blending [60] or synergistic with other ions [61], increased its hydrophilicity, promoted cell adhesion, cell proliferation and osteogenic differentiation of periodontal ligament cells (PDLCs), bone marrow stromal cells (BMSCs) and preosteoblasts [62,63]. In this study, Ca ions was successfully chelated onto the surface of PP or PP/COL I scaffolds via pDA coating with the maintenance of 3D nanofibrous electrospun architecture, elastic modulus and fracture stress. Although the deposition of calcium on the surface of the modified scaffolds would result in the loss of

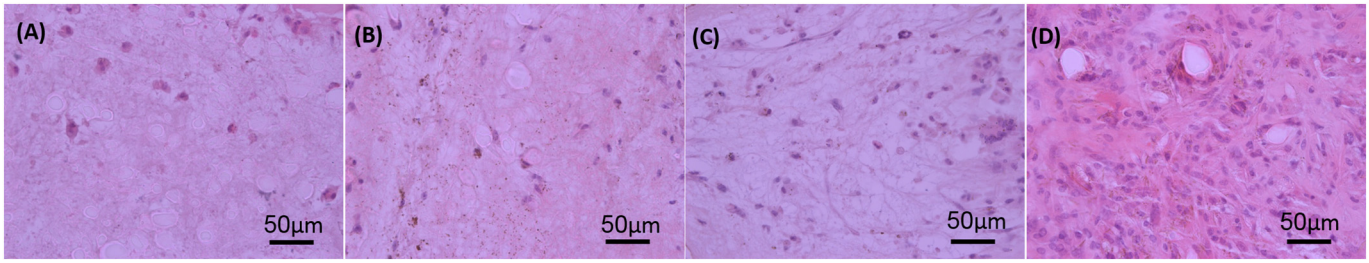

Fig. 11. Subcutaneous implantation of PP/COL I-pDA-Ca and three control scaffolds. (A-D) H&E staining. Note that much more cells penetrated into PP/COL I-pDA-Ca (D) scaffolds than PP (A), PP-pDA (B), PP-pDA-Ca (C).

hydrophilic groups, PP/COL I-pDA-Ca still exhibited better hydrophilicity due to pDA coating and type I collagen incorporation. Polydopamine coating meets the challenges of calcium incorporation into the polymer blend (PLGA/PCL/COL I) electrospun scaffold for that calcium does not necessarily need to be chemically bonded with the organic polymer scaffold to make the hybrid bioactive and osteogenic, but the dissolution rate of calcium should be congruent with other bioactive components from the hybrid biomaterial scaffolds [64]. This can be achieved by higher degree of crosslinking between organic and inorganic phases by poly-dopamine coating thus that calcium will be entrapped within the 3D architecture of electrospun scaffold. Our results demonstrated that the developed novel PP/COL I-pDA-Ca scaffolds promoted MC3T3-E1 cell adhesion, proliferation and osteogenic differentiation attributed to the immobilized Calcium onto the scaffold surface synergistically with collagen I incorporation into the basic matrix.

4. Conclusion

In this study, a favorable microenvironment for MC3T3-E1 cell adhesion, proliferation and differentiation were successfully created by chelating Ca ions onto the surface of PP/COL I scaffold via polydopamine coating. The results of CCK8, Live-dead cells and in vivo subcutaneous implantation demonstrated that the modified scaffold had good cytocompatibility. The significantly upregulated expression of integrin indicated that Ca ions probably preferred to bind to collagen I binding sites and collaborated with collagen I to promote cell adhesion. The ALP, OCN, OSX and western blot analysis further confirmed that the synergistic effect of Ca ions and collagen I increased bone cell differentiation and osteogenesis. The PP/COL I-pDA-Ca scaffolds meet the criteria for bone repairing procedure with attractive osteogenic property, good biocompatibility and biomimetic functionality. Therefore, the integration of bioactive ion, collagen and biomimic structure for local delivery could provide an effective strategy to accelerate bone repairing.

Data availability

The raw/processed data required to reproduce these findings cannot be shared at this time as the data also forms part of an ongoing study.

Declaration of Competing Interest

The authors declare no conflict of interest.

Acknowledgements

This work was supported by the National Natural Science Foundation of China [81801025, 31800843, 61821002 and 51832001], The State Key Program of National Natural Science Foundation of China [2017YFA0104302], Suzhou Science and Technology Development Project [SS2019062] and “National Tutor System” Training Program for Young Talents in Suzhou Health System.

Appendix A. Supplementary data

Supplementary data to this article can be found online at https://doi.org/10.1016/j.matdes.2020.109300.

References

[1] N. Amiryaghoubi, M. Fathi, N.N. Pesyan, M. Samiei, J. Barar, Y. Omidi, Bioactive polymeric scaffolds for osteogenic repair and bone regenerative medicine, Med. Res. Rev. 40 (5) (2020) 1833–1870.
[2] V. Karageorgiou, D. Kaplan, Porosity of 3D biomaterial scaffolds and osteogenesis, Biomaterials 26 (27) (2005) 5474–5491.
[3] A. Bharadwaz, A.C. Jayasuriya, Recent trends in the application of widely used natural and synthetic polymer nanocomposites in bone tissue regeneration, Mater. Sci. Eng. C-Mater. Biol. Appl. 110 (2020) 11698.
[4] N. Iqbal, A.S. Khan, A. Asif, M. Yar, J.W. Haycock, I.U. Rehman, Recent concepts in biodegradable polymers for tissue engineering paradigms: a critical review, Int. Mater. Rev. 64 (2) (2019) 91–126.
[5] Y.B. Zhang, X.C. Liu, L.D. Zeng, J. Zhang, J.L. Zuo, J. Zou, J.X. Ding, X.S. Chen, Polymer Fiber scaffolds for bone and cartilage tissue engineering, Adv. Funct. Mater. 29 (36) (2019) 1903279.
[6] D.P. Bhattarai, M.H. Kim, H. Park, W.H. Park, B.S. Kim, C.S. Kim, Coaxially fabricated polylactic acid electrospun nanofibrous scaffold for sequential release of tauroursodeoxycholic acid and bone morphogenic protein2 to stimulate angiogenesis and bone regeneration, Chem. Eng. J. 389 (2020) 123470.
[7] S. Kuttappan, J.I. Jo, C.K. Sabu, D. Menon, Y. Tabata, M.B. Nair, Bioinspired nanocomposite fibrous scaffold mediated delivery of ONO-1301 and BMP2 enhance bone regeneration in critical sized defect, Mater. Sci. Eng. C-Mater. Biol. Appl. 110 (2020) 110591.
[8] Z.H. Lu, S.J. Liu, Y.G. Le, Z.N. Qin, M.W. He, F.B. Xu, Y. Zhu, J.M. Zhao, C.B. Mao, L. Zheng, An injectable collagen-genipin-carbon dot hydrogel combined with photodynamic therapy to enhance chondrogenesis, Biomaterials 218 (2019) 11190.
[9] S.J. Wang, D. Jiang, Z.Z. Zhang, Y.R. Chen, Z.D. Yang, J.Y. Zhang, J.J. Shi, X. Wang, J.K. Yu, Biomimetic nanosilica-collagen scaffolds for in situ bone regeneration: toward a cell-free, one-step surgery, Adv. Mater. 31 (49) (2019) 1904341.
[10] T.E. Karpov, O.O. Peltek, A.R. Muslimov, Y.V. Tarakanchikova, T.M. Grunina, M.S. Poponova, A.S. Karyagina, R.V. Chernozem, I.O. Pariy, Y.R. Mukhortova, M.V. Zhukov, M.A. Surmeneva, M.V. Zyuzin, A.S. Timin, R.A. Surmenev, Development of optimized strategies for growth factor incorporation onto electrospun fibrous scaffolds to promote prolonged release, ACS Appl. Mater. Interfaces 12 (5) (2020) 5578–5592.
[11] Q.L. Ma, N. Jiang, S. Liang, F.L. Chen, L. Fang, X. Wang, J.J. Wang, L.H. Chen, Functionalization of a clustered TiO2 nanotubular surface with platelet derived growth factor-BB covalent modification enhances osteogenic differentiation of bone marrow mesenchymal stem cells, Biomaterials 230 (2020) 119650.
[12] J.J. Diao, H.W. Ding, M.Q. Huang, X.L. Fu, F. Zou, T.J. Li, N.R. Zhao, C.B. Mao, Y.J. Wang, Bone Defect Model Dependent Optimal Pore Sizes of 3D-Plotted Beta-Tricalcium Phosphate Scaffolds for Bone Regeneration, Small Methods 3 (11) (2019) 1900237.
[13] J.M. Sadowska, F. Wei, J. Guo, J. Guillem-Marti, Z.M. Lin, M.P. Ginebra, Y. Xiao, The effect of biomimetic calcium deficient hydroxyapatite and sintered beta-tricalcium phosphate on osteoimmune reaction and osteogenesis, Acta Biomater. 96 (2019) 605–618.
[14] A.I. Rodrigues, M.B. Oliveira, J.F. Mano, M.E. Gomes, R.L. Reis, I.B. Leonor, Combinatorial effect of silicon and calcium release from starch-based scaffolds on Osteogenic differentiation of human adipose stem cells, ACS Biomater. Sci. Eng. 1 (9) (2015) 760–770.
[15] J.S. Lee, J.C. Lee, J.S. Heo, Polydopamine-assisted BMP-2 immobilization on titanium surface enhances the osteogenic potential of periodontal ligament stem cells via integrin-mediated cell-matrix adhesion, J. Cell Commun. Signaling 12 (4) (2018) 661–672.
[16] Y.W. Chen, Y.F. Shen, C.C. Ho, J. Yu, Y.H.A. Wu, K. Wang, C.T. Shih, M.Y. Shie, Osteogenic and angiogenic potentials of the cell-laden hydrogel/mussel-inspired calcium silicate complex hierarchical porous scaffold fabricated by 3D bioprinting, Mater. Sci. Eng. C-Mater. Biol. Appl. 91 (2018) 679–687.

[17] K. Zhang, Y. Wang, T. Sun, B. Wang, H.Y. Zhang, Bioinspired surface functionalization for improving Osteogenesis of electrospun Polycaprolactone Nanofibers, Langmuir 34 (50) (2018) 15544–15550.
[18] C.T. Kao, Y.J. Chen, H.Y. Ng, A.K.X. Lee, T.H. Huang, T.F. Lin, T.T. Hsu, Surface modification of calcium silicate via mussel-inspired polydopamine and effective adsorption of extracellular matrix to promote osteogenesis differentiation for bone tissue engineering, Materials 11 (9) (2018) 1664.
[19] N. Li, G. Chen, J. Liu, Y. Xia, H.B. Chen, H. Tang, F.M. Zhang, N. Gu, Effect of surface topography and bioactive properties on early adhesion and growth behavior of mouse Preosteoblast MC3T3-E1 cells, ACS Appl. Mater. Interfaces 6 (19) (2014) 17134–17143.
[20] I.G. Kang, C.I. Park, H. Lee, H.E. Kim, S.M. Lee, Hydroxyapatite microspheres as an additive to enhance radiopacity, biocompatibility, and osteoconductivity of Poly (methyl methacrylate) Bone Cement, Materials 11 (2) (2018) 258.
[21] X.N. Lin, E.B. Hunziker, T. Liu, Q.G. Hu, Y.L. Liu, Enhanced biocompatibility and improved osteogenesis of coralline hydroxyapatite modified by bone morphogenetic protein 2 incorporated into a biomimetic coating, Mater. Sci. Eng. C-Mater. Biol. Appl. 96 (2019) 329–336.
[22] A.S. Neto, J.M.F. Ferreira, Synthetic and marine-derived porous scaffolds for bone tissue engineering, Materials 11 (9) (2018) 1702.
[23] Y.Z. Qian, H.B. Chen, Y. Xu, J.X. Yang, X.F. Zhou, F.M. Zhang, N. Gu, The preosteoblast response of electrospinning PLGA/PCL nanofibers: effects of biomimetic architecture and collagen I, Int. J. Nanomedicine 11 (2016) 4157–4171.
[24] A.R. Armiento, L.P. Hatt, G. Sanchez Rosenberg, K. Thompson, M.J. Stoddart, Functional biomaterials for bone regeneration: a lesson in complex biology, Adv. Funct. Mater. 1909874 (2020).
[25] Y.Z. Qian, X.F. Zhou, H. Sun, J.X. Yang, Y. Chen, C. Li, H.J. Wang, T. Xing, F.M. Zhang, N. Gu, Biomimetic domain-active electrospun scaffolds facilitating bone regeneration synergistically with antibacterial efficacy for bone defects, ACS Appl. Mater. Interfaces 10 (4) (2018) 3248–3259.
[26] Y. Qian, X. Zhou, F. Zhang, T.G.H. Diekwisch, X. Luan, J. Yang, Triple PLGA/PCL scaffold modification including silver impregnation, Collagen Coating, and Electrospinning Significantly Improve Biocompatibility, Antimicrobial, and Osteogenic Properties for Orofacial Tissue Regeneration, ACS Appl. Mater. Interfaces 11 (41) (2019) 37381–37396.
[27] K. Wang, F.M. Kievit, S.J. Florczyk, Z.R. Stephen, M. Zhang, 3D porous chitosan-alginate scaffolds as an in vitro model for evaluating nanoparticle-mediated tumor targeting and gene delivery to prostate Cancer, Biomacromolecules 16 (10) (2015) 3362–3372.
[28] J. Xue, J. Xie, W. Liu, Y. Xia, Electrospun Nanofibers: new concepts, Mater. Appl. Accounts Chem. Res. 50 (8) (2017) 1976–1987.
[29] S. Yang, X. Han, Y. Jia, H. Zhang, T. Tang, Hydroxypropyltrimethyl Ammonium Chloride Chitosan Functionalized-PLGA Electrospun Fibrous Membranes as Antibacterial Wound Dressing: In Vitro and In Vivo Evaluation, Polymers 9 (12) (2017) 1702.
[30] X. Jing, H.-Y. Mi, X.-C. Wang, X.-F. Peng, L.-S. Turng, Shish-kebab-structured poly(epsilon-Caprolactone) Nanofibers hierarchically decorated with chitosan poly(epsilon-Caprolactone) copolymers for bone tissue engineering, ACS Appl. Mater. Interfaces 7 (12) (2015) 6955–6965.
[31] H. Chen, Y. Qian, Y. Xia, G. Chen, Y. Dai, N. Li, F. Zhang, N. Gu, Enhanced Osteogenesis of ADSCs by the synergistic effect of aligned fibers containing collagen I, ACS Appl. Mater. Interfaces 8 (43) (2016) 29289–29297.
[32] Y. Liu, K. Ai, J. Liu, M. Deng, Y. He, L. Lu, Dopamine-melanin colloidal Nanospheres: an efficient near-infrared Photothermal therapeutic agent for in vivo Cancer therapy, Adv. Mater. 25 (9) (2013) 1353–1359.
[33] A.C. Jayasuriya, C. Shah, N.A. Ebraheim, A.H. Jayatissa, Acceleration of biomimetic mineralization to apply in bone regeneration, Biomed. Mater. 3 (1) (2008) 015003.
[34] R.K. Roeder, M.M. Sproul, C.H. Turner, Hydroxyapatite whiskers provide improved mechanical properties in reinforced polymer composites, J. Biomed. Mater. Res. A 67A (3) (2003) 801–812.
[35] S.-F. Chou, K.A. Woodrow, Relationships between mechanical properties and drug release from electrospun fibers of PCL and PLGA blends, J. Mech. Behav. Biomed. Mater. 65 (2017) 724–733.
[36] G.X. Tan, K.Y. Ouyang, L. Zhou, Y. Liu, L. Zhang, C.Y. Ning, Titanium modification by calcium ion chelated polydopamine and its cytocompatibility, J. Inorg. Mater. 30 (10) (2015) 1075–1080.
[37] K. Yang, J.S. Lee, J. Kim, Y.B. Lee, H. Shin, S.H. Um, J.B. Kim, K.I. Park, H. Lee, S.-W. Cho, Polydopamine-mediated surface modification of scaffold materials for human neural stem cell engineering, Biomaterials 33 (29) (2012) 6952–6964.
[38] B.N. Teixeira, P. Aprile, R.H. Mendonca, D.J. Kelly, R.M. da Silva Moreira Thire, Evaluation of bone marrow stem cell response to PLA scaffolds manufactured by 3D printing and coated with polydopamine and type I collagen, J. Biomed. Mater. Res. Part B 107 (1) (2019) 37–49.
[39] R. Khajavi, M. Abbasipour, A. Bahador, Electrospun biodegradable nanofibers scaffolds for bone tissue engineering, J. Appl. Polym. Sci. 133 (3) (2016) 42883.
[40] T.I. Hwang, J.I. Kim, M.K. Joshi, C.H. Park, C.S. Kim, Simultaneous regeneration of calcium lactate and cellulose into PCL nanofiber for biomedical application, Carbohydr. Polym. 212 (2019) 21–29.
[41] K. Anselme, A. Ponche, M. Bigerelle, Relative influence of surface topography and surface chemistry on cell response to bone implant materials. Part 2: biological aspects, Proce. Institut. Mech. Eng. H-J. Eng. Med. 224 (H12) (2010) 1487–1507.
[42] R.O. Hynes, Integrins: bidirectional, allosteric signaling machines, Cell 110 (6) (2002) 673–687.
[43] J. Tian, F.-J. Zhang, G.-H. Lei, Role of integrins and their ligands in osteoarthritic cartilage, Rheumatol. Int. 35 (5) (2015) 787–798.
[44] M.C. Siebers, P.J. ter Brugge, X.F. Walboomers, J.A. Jansen, Integrins as linker proteins between osteoblasts and bone replacing materials. A critical review, Biomaterials 26 (2) (2005) 137–146.
[45] R.F. Loeser, S. Sadiev, L. Tan, M.B. Goldring, Integrin expression by primary and immortalized human chondrocytes: evidence of a differential role for alpha 1 beta 1 and alpha 2 beta 1 integrins in mediating chondrocyte adhesion to types II and VI collagen, Osteoarthr. Cartil. 8 (2) (2000) 96–105.
[46] S.N. Popova, E. Lundgren-Akerlund, H. Wiig, D. Gullberg, Physiology and pathology of collagen receptors, Acta Physiol. 190 (3) (2007) 179–187.
[47] C.F. Tiger, F. Fougerousse, G. Grundstrom, T. Velling, D. Gullberg, alpha 11 beta 1 integrin is a receptor for interstitial collagens involved in cell migration and collagen reorganization on mesenchymal nonmuscle cells, Dev. Biol. 237 (1) (2001) 116–129.
[48] L. Camper, K. Holmvall, C. Wangnerud, A. Aszodi, E. Lundgren-Akerlund, Distribution of the collagen-binding integrin alpha 10 beta 1 during mouse development, Cell Tissue Res. 306 (1) (2001) 107–116.
[49] X. Zhao, Y. Han, J. Li, B. Cai, H. Gao, W. Feng, S. Li, J. Liu, D. Li, BMP-2 immobilized PLGA/hydroxyapatite fibrous scaffold via polydopamine stimulates osteoblast growth, Mater. Sci. Eng. C-Mater. Biol. Appl. 78 (2017) 658–666.
[50] J.S. Lee, J.-C. Lee, J.S. Heo, Polydopamine-assisted BMP-2 immobilization on titanium surface enhances the osteogenic potential of periodontal ligament stem cells via integrin-mediated cell-matrix adhesion, J. Cell Commun. Signaling 12 (4) (2018) 661–672.
[51] H. Wang, C. Lin, X. Zhang, K. Lin, X. Wang, S.G. Shen, Mussel-inspired Polydopamine coating: a general strategy to enhance Osteogenic differentiation and Osseointegration for diverse implants, ACS Appl. Mater. Interfaces 11 (7) (2019) 7615–7625.
[52] L.J. Chen, B.B. Hu, X.L. Shi, M.M. Ren, W.B. Yu, S.D. Cen, R.D. Hu, H. Deng, Baicalein enhances the osteogenic differentiation of human periodontal ligament cells by activating the Wnt/I beta-catenin signaling pathway, Arch. Oral Biol. 78 (2017) 100–108.
[53] J.S. Lee, J.M. Lee, G.I. Im, Electroporation-mediated transfer of Runx2 and Osterix genes to enhance osteogenesis of adipose stem cells, Biomaterials 32 (3) (2011) 760–768.
[54] S.M. Marques, P. Rico, I. Carvalho, J.L.G. Ribelles, L. Fialho, S. Lanceros-Mendez, M. Henriques, S. Carvalho, MC3T3-E1 cell response to Ti1-xAgx and Ag-TiNx electrodes deposited on piezoelectric poly(vinylidene fluoride) substrates for sensor applications, ACS Appl. Mater. Interfaces 8 (6) (2016) 4199–4207.
[55] B.W. Tillman, S.K. Yazdani, S.J. Lee, R.L. Geary, A. Atala, J.J. Yoo, The in vivo stability of electrospun polycaprolactone-collagen scaffolds in vascular reconstruction, Biomaterials 30 (4) (2009) 583–588.
[56] E. Jabbari, Osteogenic Peptides in Bone Regeneration, Curr. Pharm. Des. 19 (19) (2013) 3391–3402.
[57] L. Lao, Y. Zhu, Y. Zhang, Z. Gao, F. Zhou, L. Chen, H. Ouyang, C. Gao, Mineralization of collagen-coated electrospun poly(lactide-co-glycolide) Nanofibrous mesh to enhance growth and differentiation of osteoblasts and bone marrow Mesenchymal stem cells, Adv. Eng. Mater. 14 (4) (2012) B123–B137.
[58] Y.-L. Cheng, Y.-W. Chen, K. Wang, M.-Y. Shie, Enhanced adhesion and differentiation of human mesenchymal stem cell inside apatite-mineralized/poly(dopamine)-coated poly(epsilon-caprolactone) scaffolds by stereolithography, J. Mater. Chem. B 4 (38) (2016) 6307–6315.
[59] E.M. Valliant, F. Romer, D. Wang, D.S. McPhail, M.E. Smith, J.V. Hanna, J.R. Jones, Bioactivity in silica/poly(gamma-glutamic acid) sol-gel hybrids through calcium chelation, Acta Biomater. 9 (8) (2013) 7662–7671.
[60] Z. Ye, W. Xu, R. Shen, Y. Yan, Emulsion electrospun PLA/calcium alginate nanofibers for periodontal tissue engineering, J. Biomater. Appl. 34 (6) (2020) 763–777.
[61] N.H. Marins, B.E.J. Lee, R. Marquese Silva, A. Raghavan, N.L. Villarreal Carreno, K. Grandfield, Niobium pentoxide and hydroxyapatite particle loaded electrospun polycaprolactone/gelatin membranes for bone tissue engineering, Colloids Surfaces B-Biointerfaces 182 (2019) UNSP 110386.
[62] X. Lei, J. Gao, F. Xing, Y. Zhang, Y. Ma, G. Zhang, Comparative evaluation of the physicochemical properties of nano-hydroxyapatite/collagen and natural bone ceramic/collagen scaffolds and their osteogenesis-promoting effect on MC3T3-E1 cells, Regen. Biomater. 6 (6) (2019) 361–371.
[63] Q. Zhatig, L. Chen, B. Chen, C. Chen, J. Chang, Y. Xiao, C. Wu, F. Yan, Lithium-calcium-silicate bioceramics stimulating cementogenic/osteogenic differentiation of periodontal ligament cells and periodontal regeneration, Appl. Mater. Today 16 (2019) 375–387.
[64] N. Aslankoohi, D. Mondal, A.S. Rizkalla, K. Mequanint, Bone repair and regenerative biomaterials: towards recapitulating the microenvironment, Polymers 11 (9) (2019) 1437.